



Influence of catalyst characteristics on the formation of MWCNT agglomerates during the synthesis in a fluidized bed reactor

V.L. Kuznetsov^{a,*}, S.I. Moseenkov^a, A.V. Zavorin^a, G.V. Golubtsov^a, V.V. Goidin^a, O.S. Rabinovich^b, A.I. Malinouski^b, M.Yu. Liakh^b

^a Boreskov Institute of Catalysis, Novosibirsk, Russian Federation

^b A.V. Luikov Heat and Mass Transfer Institute, Minsk, Belarus



ARTICLE INFO

Keywords:
 Catalytic synthesis
 Multi-walled carbon nanotubes
 Fluidized-bed reactor
 Agglomerates
 Cohesion
 Clumps of multi-walled carbon nanotubes
 Flowability indicators

ABSTRACT

The problem of the loss of homogeneous fluidization and the formation of large clumps of MWCNTs during their catalytic synthesis in a fluidized bed reactor has been studied experimentally and theoretically in terms of the impact of catalyst properties and synthesis process parameters. It has been shown that two factors play the most important role in the formation of large clumps of MWCNTs, namely, the ability of high-performance catalyst to produce agglomerates of MWCNTs with high cohesion, and a high concentration of catalyst particles in the fluidized bed volume. A relationship has been established between chemical components of the catalyst, its structure and cohesive properties of the MWCNT agglomerates formed on it. An approximate semi-analytical scheme for calculating the formation and growth of large fractal agglomerates (clumps) of MWCNTs during their catalytic synthesis in a fluidized bed has been developed. This approach is based on the model of sequential coagulation of MWCNT agglomerates starting from the primary ones, and made it possible to formulate the requirements for characteristics of the catalyst and parameters of the synthesis process, which ensure homogeneous fluidization in the reactor.

1. Introduction

Carbon nanotubes, due to their unique physical and chemical properties, are becoming one of the most effective components for the rapidly developing nanotechnology [1,2]. The catalytic synthesis of multi-walled carbon nanotubes (MWCNTs) in a fluidized bed (FB) from gaseous carbon-containing precursors is currently a well-developed technology that has a number of undeniable advantages over other methods for the synthesis of MWCNTs [3–6]. The use of high-performance catalysts (capable of synthesizing up to 100 g of MWCNTs per 1 g of catalyst) makes it possible to achieve a record productivity (hundreds of grams of MWCNTs per 1 h from a reactor working zone of 0.01 m² cross-sectional area), high quality of the product having a narrow distribution of MWCNTs by diameter and number of walls, and a low catalyst content (<5% by weight). Nevertheless, despite the progress in understanding the patterns of the catalytic growth of individual nanotubes and their synthesis in FB under significant increase in its volume [7–12], a number of problems related to the design of a continuous technological process remain unresolved,

which hinders further application of the method. One of the significant problems is the loss of fluidized bed homogeneity during the synthesis. Under certain conditions determined by the type of catalyst and its amount loaded into the reactor, great indestructible clumps of MWCNT agglomerates are formed, strong pressure pulsations and jet flows appear, which ultimately lead to a sharp drop in productivity, incomplete conversion of the gaseous reagent, and a large scatter of characteristics of the synthesized MWCNTs. The task of determining the specific causes and conditions leading to the loss of homogeneity of the fluidized bed in the MWCNT catalytic synthesis reactor is important in practical terms, since avoiding these undesirable phenomena makes the process more reliable and controllable.

In addition, from a broader point of view, the inhomogeneous fluidization of nanopowders is a general problem associated with high cohesive properties of these materials. Its solution for a particular case may possibly provide a clue to others. The main reason for the formation of clumps in nanopowders is known. Due to the small size of nanoparticles, they are characterized by very high ratios of the surface area to volume, which indicate a significant predominance of the cohesion

* Corresponding author.

E-mail address: kuznet@catalysis.ru (V.L. Kuznetsov).

forces between nanoparticles over the gravity forces and drag forces in a gas flow [13,14]. As a result, the nanoparticles coalesce into clusters and agglomerates. In fact, when such powders are fluidized, one has to deal not with individual nanoparticles, but with their agglomerates. Primary agglomerates of nanotubes have also strong cohesion to each other, so that their further “sticking”, enlargement and formation of secondary agglomerates occur. The growth and destruction of agglomerates due to their collisions is a dynamic process. As the nanotube agglomerates grow, the role of the surface interaction of the agglomerates decreases. Their final size and the behavior of the FB in general depend on the conditions under which the collisions and hydrodynamic forces destroying the agglomerates can balance the cohesion forces [14]. The fluidization behavior for the thus formed agglomerates of multi-walled carbon nanotubes correspond to the boundary between the C and A groups on the classical Geldart diagram [15]. Therefore, the determination of the conditions and the formation patterns of inhomogeneities in a fluidized bed for a particular process under consideration can be a source of important general information to be used for improving other technological processes with nanopowders.

The aim of this work is to formulate the conditions for maintaining homogeneous fluidization during the catalytic synthesis of MWCNTs in the form of requirements for the characteristics of the catalyst and important parameters of this technological process. This work combines experimental and theoretical approaches. The first approach is to study experimentally the relationship between properties of the catalysts and cohesive characteristics of the synthesized nanotubes with the aim of choosing the most adequate characteristic of the cohesiveness of the material. The second approach is to construct theoretical models describing the formation of large MWCNT clumps (clusters) leading to the loss of the FB homogeneity. The growth dynamics of MWCNT agglomerates and the formation of their large clusters, which cannot be in a fluidizing state, were investigated using a coagulation model. Ultimately, this model allowed estimating the critical concentration of the initial catalyst particles per unit volume of the fluidized bed at which such large clusters can form, leading to the loss of homogeneity of the MWCNT fluidized bed. Three types of catalysts with the same type of active sites (Fe-Co alloys) were taken as the objects of study. The catalysts provide the production of MWCNTs with different average diameters (~7, 10, 20 nm). These MWCNTs were obtained in recent years at the Boreskov Institute of Catalysis [16] and are widely used as a system set for studying the properties of MWCNTs [17–24], as well as the properties of composites based on them (see [25–32]). The motivation for such studies is supported by the fact that, due to a significant change in the properties of MWCNTs depending on their structure (average diameter, defectiveness, aspect ratio, functional surface composition), it is necessary to use a system set of nanotubes in the development of each individual type of composite, based on this nanotube type in order to optimize its properties for specific applications.

2. Experimental

2.1. Catalyst synthesis

In the study, three types of catalysts were used: K-1 – 30% Fe₂Co/Al₂O₃ (batch numbers 13 and 15), K-2 – 40% Fe₂Co/Al₂O₃ (batch numbers 59–65), and K-3 – 40% Fe₂Co/CaO (batch numbers 19 and 20), which provide MWCNTs with varying average diameters (~ 7, 10, and 20 nm, respectively). These Fe–Co oxide catalysts with two types of supports (Al₂O₃ and CaCO₃) were produced via the polymerized complex route based on the Pechini-type method [33–35]. Water solutions of metal nitrates (Fe, Co, Al, and/or Ca) were mixed with citric acid and ethylene glycol. These mixtures were dried at 150 °C to produce 3D polymer matrix foam with metal ions distributed in the bulk. The subsequent heating of the dried foam in air flow up to 550 °C results in the removal of organic matrix to give highly dispersed oxide systems containing homogeneously distributed metal ions of active components (Fe:

Co = 2:1) and supports. By changing the type of support (Al₂O₃, CaCO₃) and the content of active component [35] it was possible to control the particle size of the active component, providing MWCNTs with different average diameters, catalyst particles morphology and bulk density. In addition, we used different fractions of catalyst particles (with varying size and bulk density), which affect the size of the primary agglomerates of MWCNTs growing on an individual catalyst particle.

2.2. MWCNT synthesis

MWCNT were grown using CCVD technique in the reaction mixture of C₂H₄ and Ar (50:50) at 650–670 °C with Fe–Co catalysts. Further in the text, the following designations are used for the types of nanotubes studied: in the record **M-a b**, **M** means MWCNTs, **a** – type of the catalyst used for their production, and **b** – the catalyst batch number (thus, M-2 60 means MWCNTs produced with K-2 60 catalyst). Two types of reactors were used. The first is a fixed bed tubular flow reactor for preliminary 15 min catalyst activity tests. In the test, a 50 mg of catalyst was placed in a horizontal quartz tube of 4 cm diameter with a gas flow of C₂H₄:Ar mixture at 670 °C; the catalyst productivity I₁₅ was determined as the amount of MWCNTs obtained from 1 g of the catalyst for 15 min of the synthesis [11]. The second is a fluidized bed reactor (FBR) with diameter 120 mm and height 2500 mm, having an expanded section at the top, equipped with a preheater, a powder catalyst loading unit, and four valves allowing the withdrawal of nanotubes during the reaction from different height levels of the reactor. Uniformity of the temperature field in FBR was provided by 4-section heating of the reactor. The bed pressure drop in FBR was measured during the MWCNT synthesis with an electronic digital manometer. We used this reactor to evaluate the tendency to form clumps under reaction conditions, and to simulate and optimize the FB reactor operation under continuous cycling. The catalyst amount loaded and the duration of MWCNT synthesis and loading cycles were optimized using experimental data obtained in a fixed bed reactor, as discussed by us in [10,11].

The use of highly reactive catalysts in FB reactor imposes a number of technological problems, not the least of which is the prevention of overheating due to the exothermic reaction of MWCNTs formation from ethylene. Overheating can lead to deterioration in the product quality and disruptions of the technological process (an increased width of nanotube diameter distribution, an increased mass of lateral deposits, catalyst deactivation [12,35,36], formation of clumps leading to poor fluidization, and formation of dome-shaped sheets on the walls of the separation zone, which can fall back into the reactor). Local overheating of the fluidized bed can occur when the catalyst is not uniformly distributed in it. For this reason, it is necessary to avoid loading large portions of the catalyst into the reactor. The situation is somewhat similar to that arising in fluidized bed reactors designed for catalytic polymerization [37]. So, we used the following procedure for the cyclic process of catalytic synthesis of carbon nanotubes in a FB reactor [10,11]:

(i) A certain amount of MWCNTs is initially loaded into the reactor (to fill the bottom of the reactor space in order to avoid overheating and organize the primary FB);

(ii) A catalyst is added stepwise, in small portions separated in time to ensure its uniform distribution in the reactor and gradual activation, and the MWCNT synthesis starts;

(iii) After the nanotubes have filled almost the entire volume of the reactor, most of the product containing MWCNTs with partially deactivated catalyst is discharged through one of the valves to the level corresponding to the initial reactor loading; the output is about 30–70 g MWCNTs per 1 g of catalyst, depending on the catalyst type;

(iv) The portion of a fresh catalyst is loaded into the reactor, and the process is repeated as successive cycles of CNT synthesis and reactor reloading (SR cycles).

2.3. Catalyst and MWCNT powders characterization

Catalyst and MWCNT powders were characterized using optical transmission and reflection microscopy (Micromed POLAR 1, Russia) and scanning electron microscopy (SEM, JSM6460-LV JEOL and SU8230 Hitachi, Japan). The structure of catalysts and MWCNTs was also characterized with transmission electron microscopy (TEM, JEM 2010 Jeol). For TEM characterization of the specimen structure, a sample was deposited on a copper grid with a carbon film. Nanotube average diameters were estimated from several low magnification TEM images taken at 100,000X magnification. The specific surface area (S_{BET}) of the samples was monitored using N_2 adsorption isotherms (77 K) obtained with the surface area and porosimetry analyzer ASAP-2400 (Micromeritics, USA).

2.4. Powder flowability indicators

Determination of the main parameter that adequately characterizes the tendency of nanopowder to form clumps in a fluidized bed is an important element of research. Traditional flowability indicators, including Hausner ratio (HR), angle of repose, avalanche angle and index of cohesion, were tested in the paper. Tapped and bulk densities of the catalyst and MWCNT powder were measured to find their ratio (HR) [38] in accordance with the procedure described in ASTM D7481-09 [39]. The true density was estimated using a helium pycnometer (Quantachrome Instruments, Ultrapyc 1200e V4.02). The angle of repose was measured for each MWCNT powder in accordance with the standardized testing procedures, where a powder flows freely through a funnel and onto a circular plate to form a conical heap (ISO 4490:2014). The avalanche and overhang angles as well as the index of cohesion for MWCNT powders were measured using a drum rheometer consisting of a rotating drum (angular frequency of 0–120 min⁻¹, an inner diameter of 108 mm and a width of 50 mm) and a camera recording the dynamic distribution of MWCNT powders in the drum. The analysis of powder profiles at various rotation velocities was carried out with ImageJ software (LOCI, University of Wisconsin).

3. Results and discussion

3.1. Catalytic properties of Fe-Co catalysts

The structure and evolution of Fe-Co catalysts under the reaction conditions were studied in detail in [35]. The initial catalysts K-1 and K-2 contained highly dispersed spinel-like phases based on Co, Fe and Al oxides, namely, $CoFe_2O_4$, $Co(Fe^{2+})Al_2O_4$ and Fe_3O_4 . K-3 contains mainly $CoFe_2O_4$ and $CaCO_3$ (it decomposes to CaO under the reaction conditions). We have employed *in situ* activation of the catalyst (i.e. the reduction of metals from metal oxides by ethylene in the reaction mixture gas flow) to provide the formation of MWCNTs with a narrow diameter distribution owing to the lower critical size of carbon nucleus [9]. In the course of activation due to the reduction of oxides with ethylene, the formation of Fe-Co alloy particles, which are highly active in the synthesis of MWCNTs, occurs [35]. The kinetics of the metal reduction from Fe-Co oxides and growth of MWCNTs is given in [11]. ^{59}Co IF NMR provided original information with regards to the evolution of metal catalysts structure and composition during the activation process [40]. By ^{59}Co IF NMR, in a sample of the initial composition $CoFe_2O_4$, the following sequence of events could be clearly identified. Cobalt was reduced first when the bimetallic precursor was activated under reaction conditions. It then catalyzed the release of hydrogen from the ethylene feed decomposition and the activated hydrogen further reduced the Fe oxide. Thus, first, a strong ferromagnetic Co-Fe alloy is formed, followed by its ordering and diffusion of metallic Co into the volume of reduced Fe with the formation of a weakly ferromagnetic Co-Fe alloy. Finally, the ordering process evidenced by ^{59}Co IF NMR is expected to play a role in carbon nucleation and favor the onset

of the MWCNT intensive growth at the end of the induction period. Over time, the catalysts are deactivated due to the dissipation of the active component in the internal channels of the nanotubes.

The fresh catalyst goes through the activation stage, i.e. the reduction of metals from their oxides, within approximately 2 min after loading into the reactor. Then the growth of nanotubes begins, the mass of which initially increases linearly with time, but, after about 15–20 min, the growth rate begins gradually to slow down due to the encapsulation of catalyst nanoparticles inside growing nanotubes.

Data on the properties of the studied catalysts and the MWCNTs obtained on them, including their tendency to form clumps, are collected in Table 1. Typical TEM images of MWCNTs obtained using different types of catalysts, as well as the corresponding diameter distributions of MWCNTs, are shown in Fig. S1. Data of the catalyst 15-min test demonstrate that the MWCNT yield varies in the range of 19–30 g/1 g of catalyst (during this time). K-2 catalysts are the most active. The total mass of the catalyst loaded in a single cycle by small fractional portions into the FB reactor was the same in all the experiments under consideration and amounted to 5 g. The optimal time of SR cycles was determined by the method described in [11], while trying to ensure a high efficiency of C_2H_4 use and a low content of catalyst traces (<3%). With the target production of MWCNTs with certain parameters, the daily productivity of the used pilot reactor with an internal diameter of 120 mm can be increased for M-1 up to 8 kg, for M-2 up to 10 kg, and for M-3 up to 6 kg by increasing the catalyst load and cycle time.

The tendency to clump formation in the FB reactor for different catalysts was estimated during repeated cycles. As the main criterion for stability of the FB reactor (related to the cohesiveness of nanotubes in the FB) we used the “tendency to form clumps under conditions of MWCNT synthesis in the FB reactor” (see Table 1). “Low” corresponds to the stable operation of the reactor ensuring more than 30 cycles of SR without stopping the process and cleaning the reactor. “Moderate” – the reactor operated steadily (up to 25–30 SR cycles). At a “High” tendency to clumping, the reactor was clogged after 1–3 SR cycles.

As can be seen from Table 1, in the last two experiments, the formed MWCNTs show the greatest tendency to form clumps. In the first of them, a finely dispersed fraction of catalyst K-2 with a particle size of < 40 μm (the average size of about 20 μm) was used, while in the second, a catalyst K-3 prepared on a support $CaCO_3$, which is easily crushed under the reaction conditions. The role of these features will be analyzed further.

Fig. 1 presents typical protocols of FB testing of catalysts related to the tendency to clump formation in a FB reactor. The dependences of the temperature and fluidized bed pressure drop on the synthesis time were obtained for different types of catalysts and different catalyst loading procedures. The variation of pressure drops in the FB at the beginning of each cycle corresponds to the stepwise loading of the catalyst, during which small portions of the catalyst from the dispenser were injected into the lower part of the reactor. The catalysts less prone to clump formation in a FB reactor showed a monotonic increase in the pressure drop in the reactor during MWCNT growth in each SR cycle (catalyst K-2 60). Reducing the portions of the introduced catalyst at the loading stage (keeping constant the total amount of catalyst loaded in one cycle) ensures a more uniform increase in the pressure drop in FB reactor (the effect of increasing the number of portions of the loaded K-2 60 catalyst from 6 to 20 is shown in Fig. 1, two fragments on the right). The formation of clumps leads to a decrease in the reactor pressure drop. Thus, catalysts K-2 59 and K-3 19 (Fig. 1) demonstrate a low pressure drop and low MWCNT yields even after early SR cycles (in 4th and 1st cycles respectively).

To understand the tendency to clump formation, we carried out an accurate study on the structure and morphology of the catalysts and MWCNT powders as well as the parameters characterizing their flowability. Note that the K-2 60 catalyst with a fractional composition of 40–80 μm ensured stable operation of FB reactor.

The change in the reactor temperature during the synthesis of

Table 1

Properties of Fe-Co catalysts and MWCNTs synthesized on them.

Catalyst (type, batch number)	Bulk catalyst density, g/cm ³ /surface area(BET) m ² /g	FIXED BED REACTOR. Yield of MWCNTs in 15 min test, g _{MWCNT} /1g of catalyst	FLUIDIZED BED REACTOR. Mean yield of MWCNTs in SR cycles, g _{MWCNT} /1g of catalyst/cycle time, min	MWCNTs average diameter, nm	MWCNT surface area (BET), m ² /g	**Tendency to clump formation in FB reactor
K-1, 30 % Fe ₂ Co/Al ₂ O ₃ -13	0.25/172	19.8	32.5 ± 2.5/40	7 ± 0.2	350 ± 15	Low
K-1, 30 % Fe ₂ Co/Al ₂ O ₃ -15	0.29/180	22.0	35.5 ± 2.5/40	7 ± 0.2	360 ± 15	Low
K-2, 40 % Fe ₂ Co/Al ₂ O ₃ -59	0.41/232	21.6	40 ± 2.5/50	10 ± 0.3	250 ± 10	Moderate
K-2, 40 % Fe ₂ Co/Al ₂ O ₃ -60	0.412/252	29.3	45 ± 2.5/40	10 ± 0.3	245 ± 10	Moderate
K-2, 40 % Fe ₂ Co/Al ₂ O ₃ -63 (40–80 µm)	0.554	29	42 ± 3/45	10 ± 0.3	245 ± 10	Moderate
K-2, 40 % Fe ₂ Co/Al ₂ O ₃ -65 (40–80 µm)	0.292/236	30.5	57 ± 3/50	10 ± 0.3	245 ± 10	Low
K-2, 40 % Fe ₂ Co/Al ₂ O ₃ -65 (<40 µm)	0.222/243	31	n/a	10 ± 0.3	—	Ext. high
K-3, 40% Fe ₂ Co/CaO-19	0.34/56	19.2	30±3/40	19 ± 0.4	115 ± 5	High

* 15 min test in a fixed bed reactor at 670 °C;

** “Low” corresponds to the stable operation of the reactor providing more than 30 SR cycles without stopping the process and cleaning the reactor. “Moderate” – the reactor operated steadily up to 25–30 SR cycles. At a “High” tendency to clumping, the reactor was clogged after 1–3 SR cycles.

MWCNTs on various catalysts is also shown in Fig. 1 (upper curves). It is impossible to resolve temperature changes in time at the stage of catalyst activation and at the stage of subsequent MWCNT growth, since the activation is not synchronous at different points of the reactor and the temperature field in the reactor is quite inertial (the catalyst activation time about 120 s is short compared to the recorded temperature fluctuations). Temperature fluctuations are mainly caused by the inertia of the heater. With stable operation of the reactor, they do not exceed ± 5 °C.

The temperature conditions of the FB reactor are analyzed in detail in the article [10]. The temperature in the reactor can rise precisely in the initial period after loading and activation of the catalyst, when the synthesis proceeds most rapidly and this is one of the reasons for using fractional loads. The effect of catalyst overheating on the average nanotube diameter and amorphous carbon formation was analyzed in [36].

3.2. A comparison of the morphologies of different catalysts and MWCNTs synthesized on them

Figs. 2 and 3 present optical microscopy and SEM images of the catalyst powders produced using Al₂O₃ and CaCO₃ (K-1 and K-3, respectively).

Particles of the catalysts K-1(2) have a shape close to the typical fragments of polydisperse foam (curved films, plateau boundaries, and tops). At the same time, due to its specific morphology, the K-3 catalyst (see Fig. 3 B) has a fractal structure and consists of fragments of a relatively big particle of the support (CaCO₃) and small particles of Fe-Co spinel (CoFe₂O₄).

Fig. 4 shows a series of electron microscope images demonstrating the structure of primary agglomerates of MWCNTs formed on the K-2 catalyst. Note that similar images, reflecting the generality of the formation mechanism, were obtained for other types of catalysts. During the *in situ* activation of catalyst particles, numerous nano-sized active

centers (Fe-Co alloy) are formed on the support surface [17]. This leads to the multicenter growth of entangled MWCNTs. Due to entanglement of the growing MWCNTs, a rather rigid openwork structure of their primary agglomerates is formed. According to our estimates (see Section 3.3), during the synthesis, the growing MWCNTs form particles (agglomerates) with a volume exceeding the volume of the initial catalyst particles by more than 400 times. During the growth of MWCNTs, the catalyst particles are broken into smaller primary particles corresponding to the size of the primary particles of the original catalyst support. These particles become covered with growing nanotubes. Their combination provides multiple strained contacts between nanotubes growing from different centers, which, in turn, cause the formation of a rigid openwork structure of the material.

Figs. 5 and 6 show the difference in the morphology of MWCNT agglomerates produced with different catalysts (K-1(2) and K-3).

It can be seen that the shape of the primary MWCNT agglomerates for catalysts K-1 and K-2 approximately corresponds to the shape of the catalyst particles used with a dramatic increase in their volume. Shape analysis of the fixed bed and FB agglomerates suggests that the primary agglomerates in FB have a more rounded particle shape due to multiple collisions of the growing particles. At the same time, for both types of reactors, the formation of entangled bundles of nanotubes is observed on MWCNT agglomerates. In contrast, the catalysts K-3 give a broad particle size distribution of primary MWCNT agglomerates (see Fig. 6 A-C). Moreover, the surface of these agglomerates consists of chaotically entangled nanotubes. The difference in the morphology of the primary agglomerates indicates that catalysts K-3 decompose into smaller fragments upon activation, which leads to a significant increase in the number of growing nanotube agglomerates. This process is schematically presented in Fig. 6D. This assumption is confirmed by the fractal structure of catalyst K-3, which consists of coarse CaCO₃ particles coated with relatively smaller Fe-Co spinel particles (Fig. 3B). These fractal structures seem to be able to easily disintegrate to form a wide variety of small growing primary agglomerates, which appear to have an increased

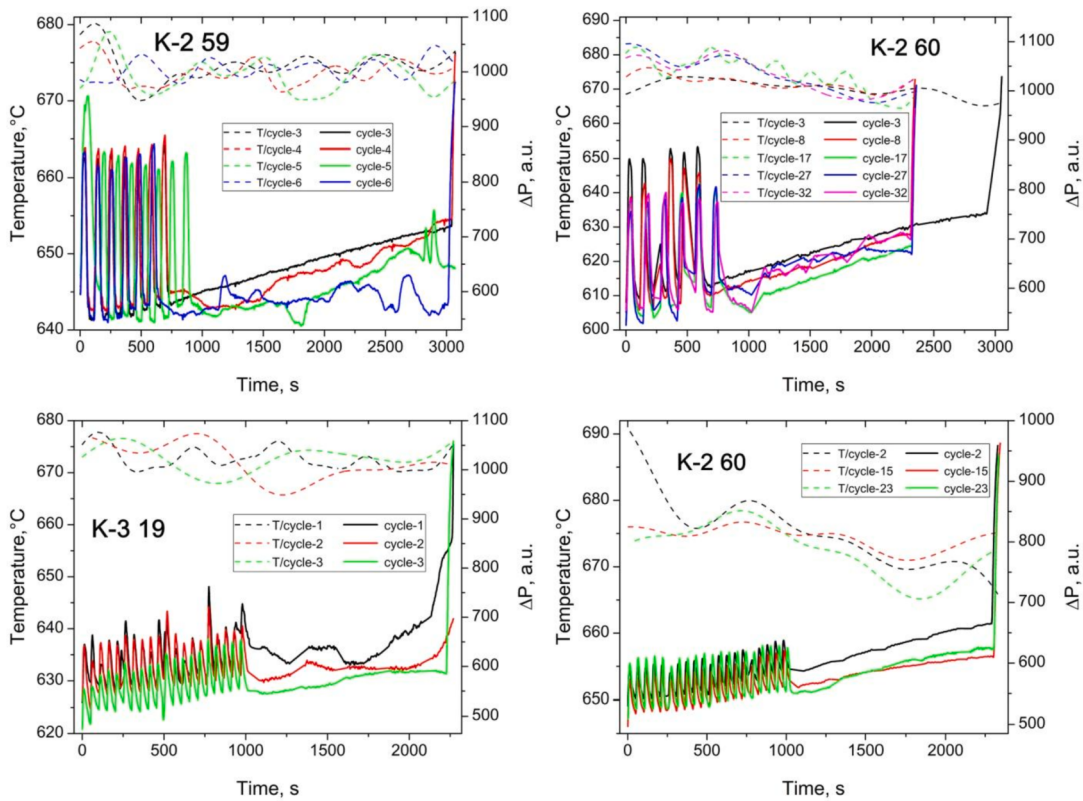


Fig. 1. Dependences of temperature (dashed upper curves) and pressure drop in the fluidized bed (lower curves) on the synthesis time obtained for different types of catalysts (K-2 59, K-3 19 and K-2 60) for different successive SR cycles (see inserts for the sequence number of the cycles). Pulsations of the pressure drop in the FB at the beginning of each cycle correspond to the stepwise loading of the catalyst (the introduction of each portion of the catalyst by injection from the dispenser into the lower part of the reactor is accompanied by a short-term increase in the pressure drop). Two right figures correspond to different methods of catalyst loading for K-2 60 (for the upper figure the catalyst loading was carried out in 6 portions for the bottom one, in 20 portions) corresponding to the selected SR cycles.

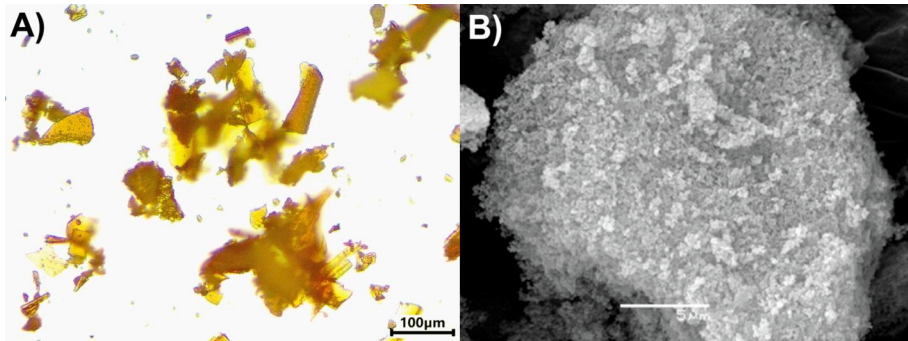


Fig. 2. A) Optical microscope image of the K-1 catalyst (as produced, fraction 40–80 μm); B) typical SEM image of the K1 catalyst surface. (K-2 catalysts have a similar morphology, but are somewhat more colored due to the higher content of Fe-Co active components).

ability to form clumps due to a higher probability of primary agglomerate collision with each other.

3.3. Estimated volume distribution of the catalysts

The results obtained with catalyst K-3, indicating its destruction in the FB, led us to the necessity of experiments for studying the effect of the number of growth centers (catalytic particles) per unit volume of the reactor on the FB stability. Thus, we estimated the particle volume distribution of several K-2 catalysts from the optical and scanning electron microscopy data demonstrating different tendency to clump formation in FB reactor. Images of the catalyst powders obtained with an optical microscope Micromed Polar (Russia), SEM, and ImageJ software were used for the analysis of particle size distribution. Typical images

and the particle analysis procedure are presented in Fig. 7. The volume particle distribution was obtained using the oval approximation of particle cross-section (S_i) based on digital optical microscopy images (Fig. 7, A-B) and average particle thickness $H(S_i)$ estimated using SEM images (Fig. 7, C with the inserted graph) obtained for different size particles at different tilt angles:

$$\sum V_i = \sum (S_i \cdot H(S_i)) \quad (1)$$

According to our estimates, the accuracy of determining the particle size distribution was no worse than 20%. The inset in Fig. 7D shows the results of calculating the number of particles per unit fractional load (0.5 g) of catalysts K-2 with different fractional composition (40–80 μm for K-2 63 (64) as well as K-2 64 with a size < 40 μm). The measured

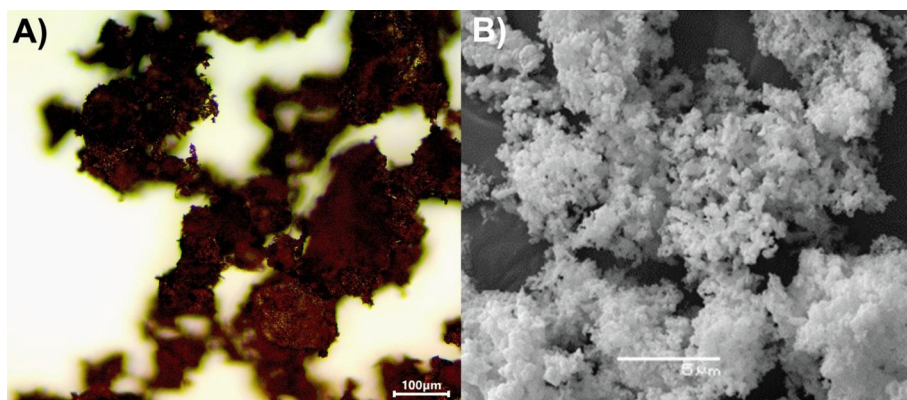


Fig. 3. A) Optical microscope image of the K-3 catalyst powder (as produced, fraction 40–80 μm); B) typical SEM image of the K-3 catalyst surface.

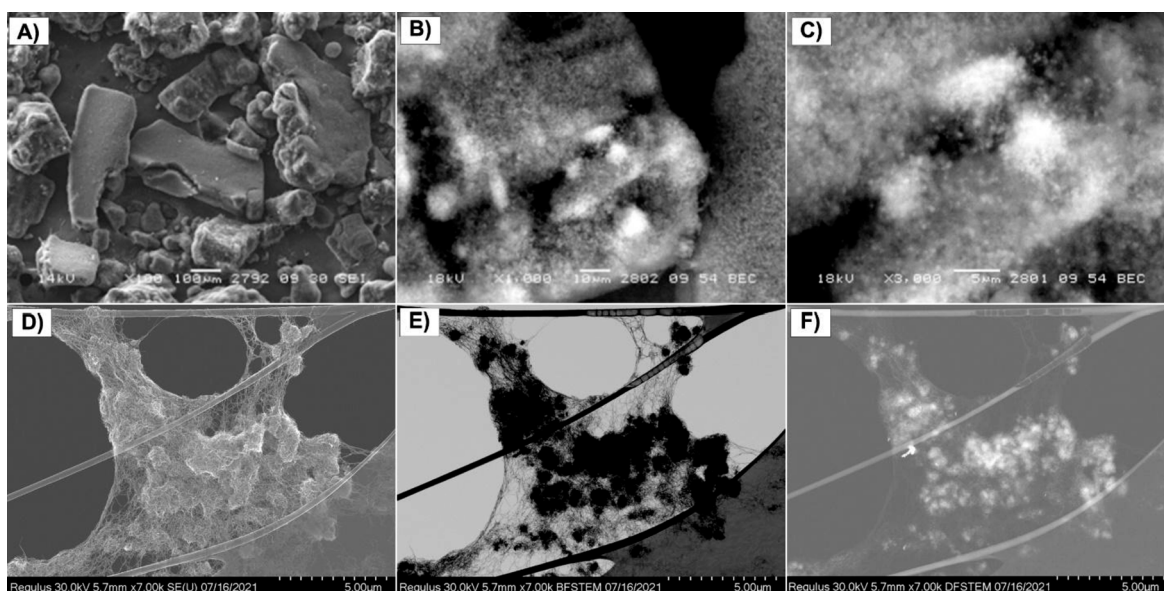


Fig. 4. Electron microscopy data for MWCNT agglomerates produced with the K-2 catalyst. A) Low magnification SEM image of MWCNTs; B) and C) images obtained in backscattered electrons confirmed the presence of regions enriched with Fe-Co particles (bright fragments); D-F images display the same fragment of the primary agglomerate in SEM, bright and dark field STEM modes, respectively.

pycnometric density of the catalyst was used to estimate the number of particles per unit weight of the catalysts. The number of particles in the fine fraction of catalyst K-2 64 ($\sim 20 \mu\text{m}$) is an order of magnitude higher than the number of particles of this catalyst in the fraction of 40–80 μm . With the same weight loading of the catalysts, the difference in the particle size distribution produced a very strong effect on the FB stability and homogeneity. So, when using the K-2 64 fraction with a diameter of $\sim 20 \mu\text{m}$, the formation of clumps was observed already in the first cycle of the reactor operation.

To ensure stable operation of the reactor in the case of a K-3 type catalyst producing agglomerates of MWCNTs with a very high cohesion, we used preliminary deposition of the catalyst particles on M-3 nanotube powders obtained in independent experiments using this type of catalyst. The K-3 and M-3 powders (1: 1 by weight, in Fig. 8 and Table 2 the sample mentioned as K-3 20 + MWCNTs (mixed)) were mixed in a knife mill at 1000 rpm within 2 min. Fig. 8 displays SEM images of the catalyst K-3 distributed on the surface of M-3 agglomerates. The use of catalyst K-3, which was previously distributed on the surface of M-3 agglomerates, provided a stable operating mode of the FB reactor (more than 25 SR cycles without complete reloading and cleaning of the reactor). Thus, the preliminary distribution of the catalyst on the surface of MWCNT agglomerates seems to limit both the decomposition of

catalyst particles upon its activation under FB conditions and the number of growing primary MWCNT agglomerates.

3.4. Analysis of the catalyst and MWCNT powders flowability indicators

3.4.1. Hausner ratio

Hausner ratio (HR) is traditionally used to describe the packing behavior and flowability of powders [41–43]. It was proposed that powders with $\text{HR} \leq 1.25$ are considered as free flowing, while cohesive and nonflowing powders have HR greater than 1.40. It should be noted that for the powders studied by us, this parameter showed a low sensitivity. Almost all powders of the catalysts and MWCNTs obtained with their use were characterized by HR greater than 1.4, which implies their high cohesion, low flowability and provides certain difficulties for creating a stable FB (see Table 2). At the same time, only the MWCNTs obtained using catalyst K-3 showed an increased tendency to form clumps. For such MWCNTs, the highest (1.73) HR value was obtained.

3.4.2. Angles of repose

Angles of repose data are listed in Table 3. The obtained values ($44-50^\circ$) are typical of the powders with high cohesion. However, the measurement accuracy does not allow unambiguous conclusions for a

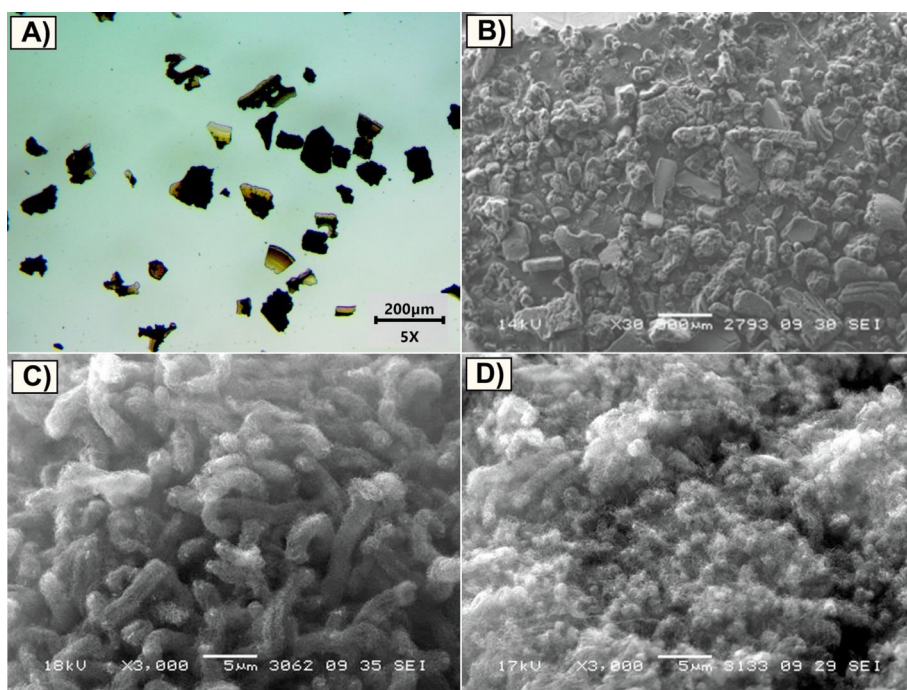


Fig. 5. A) Optical microscope image of the catalyst particles (K-2); B) low magnification SEM image of MWCNTs produced with the K-2 catalyst; C and D are typical SEM images of the surface morphology of primary MCWNT agglomerates obtained using catalysts K-1 and K-2, respectively.

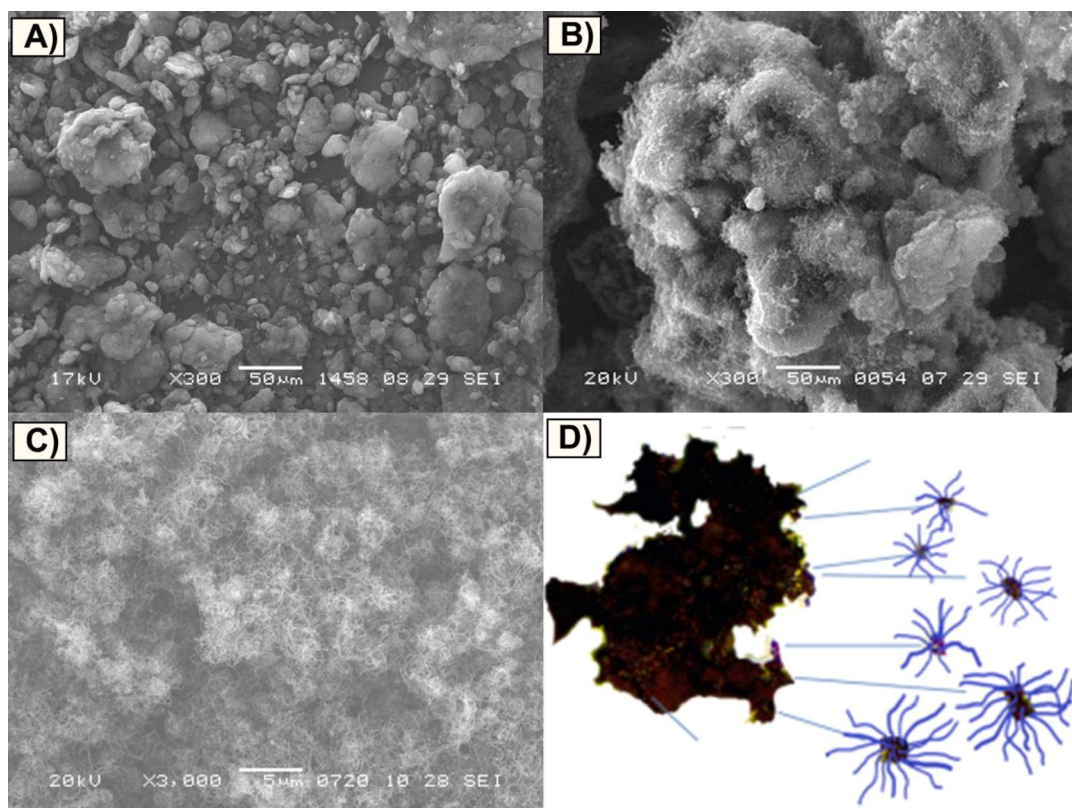


Fig. 6. A) SEM image shows the morphology of MWCNT agglomerates produced with the K-3 catalyst; B) and C) SEM images of the surface morphology of the primary MWCTN agglomerate (K-3 catalyst); D) the decomposition scheme of the K-3 catalyst particle upon activation under reaction conditions into a large number of smaller particles, providing a significant growth and an increase in the particle size distribution of the primary MWCNT aggregates.

comparative analysis of the flowability of MWCNTs obtained using different catalysts. At the same time, the highest values of the angle of repose were observed for MWCNTs obtained with the use of catalyst K-3,

which provides the most unstable FB due to the formation of clumps (see Table 1).

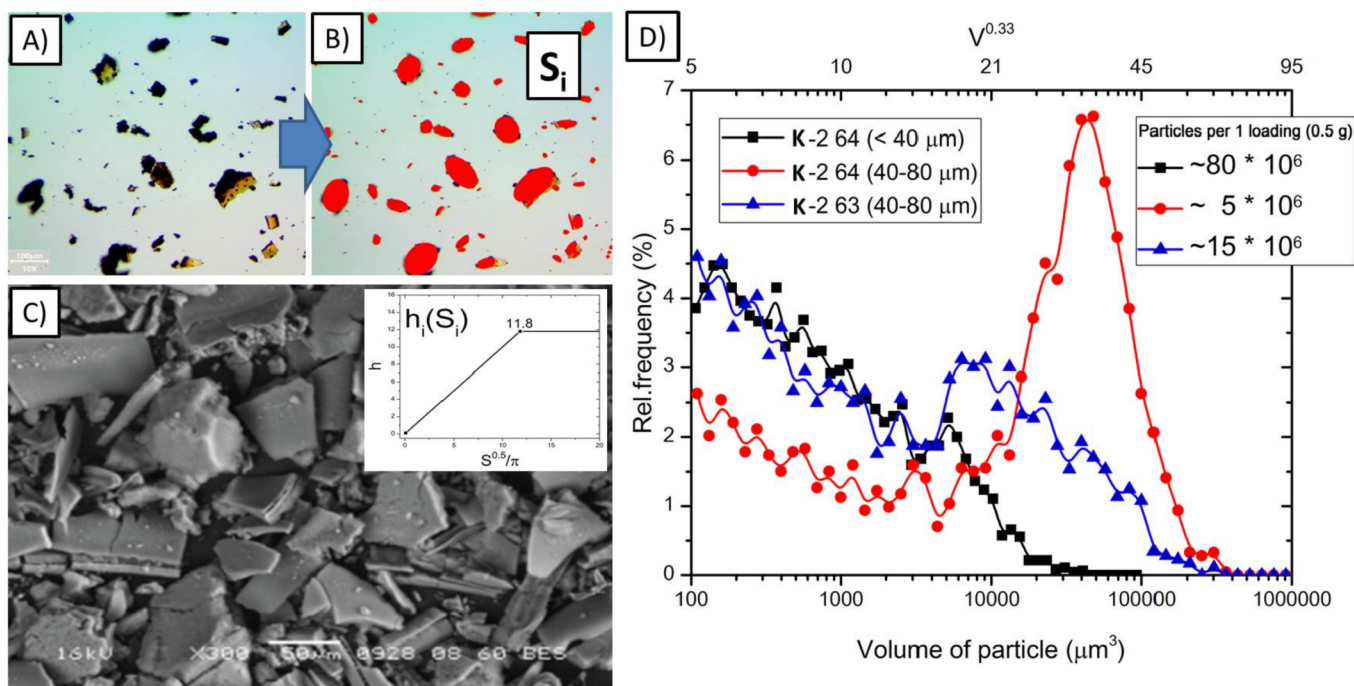


Fig. 7. Calculation of the size (volume) distribution of K-2 catalyst particles according to optical and scanning electron microscopy data. A), B) approximation of the cross-section of catalyst particles; C) estimation of the function of particles thickness versus the cross-section of catalyst particles; D) volumetric distribution of catalyst particles and the number of particles per one loading portion (0.5 g).

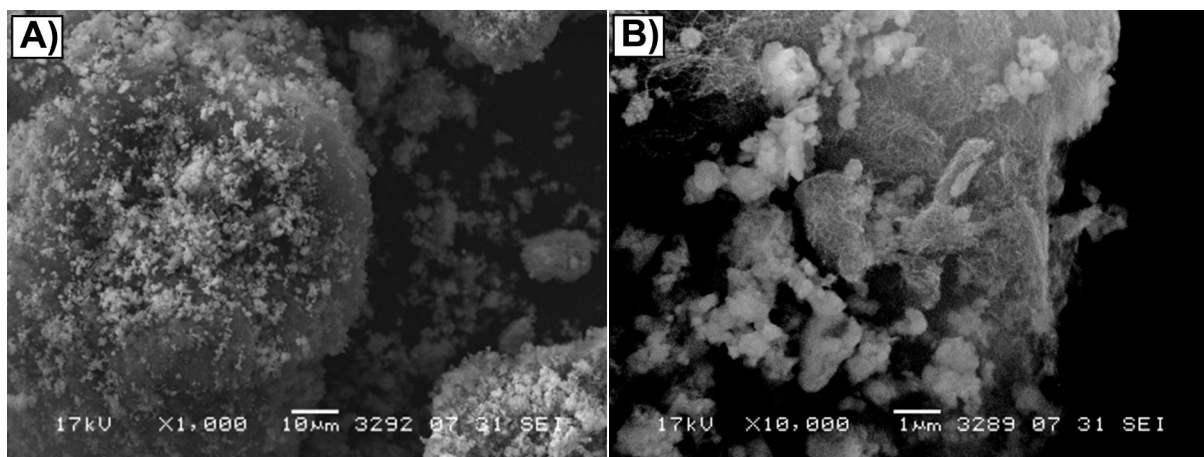


Fig. 8. SEM images of the K-3 20 catalyst particles deposited on MWCNTs (K-3 20 + MWCNTs (mixed)). Bright images of the catalyst particles with the size near 1 μm and less are clearly seen on the surface of primary MWCNT agglomerates.

3.4.3. Drum rheometer experiments

The study of the dynamic characteristics of MWCNT powders was carried out using a drum rheometer (see description in the Section on powder characterization). The behavior of the MWCNT powder layer depending on the drum rotation speed was videorecorded and analyzed using the ImageJ and Gdrum (our own development) software packages. Three effects of the drum rotation speed on the following parameters of MWCNT powders have been analyzed: 1) the value of the angles of avalanche and overhang; 2) the time between avalanches; and 3) the cohesion index.

To determine the time between avalanches, the avalanche and overhang angles in the profile of the powder-air interface, the following areas were identified: 1) the avalanche angle of the powder, 2) the overhang angle of the powder (Fig. 9A), and their change with time at a fixed drum rotation speed (Fig. 9B).

It was found that at low drum rotation speeds (0.24–0.41 rpm),

MWCNTs forming large clumps in FB are characterized by a 45–50% increase in the average time between avalanches as compared to MWCNT samples forming a stable FB (Fig. 10). At the same time, these samples are also characterized by an increase in the angles of avalanche and overhang to 80° and 45° versus, respectively, 60° and 15° for the samples forming a stable FB. For clumping MWCNTs, the layer turns out to be stable at high values of the angles of avalanche and overhang due to higher cohesive forces. MWCNTs forming a stable fluidized bed (according to the operation data of the reactor with FB (see Table 1)) show avalanches sliding down a layer of small-volume agglomerates. For such MWCNT powders, smaller values of overhang angles and times are observed.

With an increase in the drum rotation speed, a decrease in the time between avalanches is observed for all the samples (Fig. 10, A). At the same time, the avalanche and overhang angles for MWCNT powders with a higher cohesion virtually do not change at a rotation speed below

Table 2

Data on the bulk density, tapped density and Hausner ratio of catalyst and MWCNT powders.

N	Sample	Bulk density, g/cm ³	Tapped density, g/cm ³	Hausner ratio	Stability of FB
Catalysts					
1	K-2 65 (40–80 mcm)	0.207	0.292	1.41	N/A
2	K-2 65 (<20 mcm)	0.1445	0.222	1.55	N/A
3	K-3 20	0.1379	0.194	1.41	N/A
4	K-3 20 + MWCNTs (mixed)	0.186	0.320	1.72	N/A
MWCNTs produced with the catalysts					
5	M-2 60	0.031	0.049	1.57	Moderate FB
6	M-2 63	0.064	0.107	1.67	Moderate FB
7	M-2 64	0.098	0.145	1.48	Stable FB
8	M-2 65	0.096	0.141	1.46	Stable FB
11	M-3 20	0.035	0.061	1.73	Unstable FB
12	K-3 20 + MWCNTs (mixed)	0.045	0.064	1.43	Stable FB

* FB stability was assessed from the tendency for clump formation in the FB reactor (see Table 1).

Table 3

Angles of repose for different types of MWCNTs.

MWCNT type	Angle of repose, °	Reactor type used for MWCNT production
M-1 14	50	FB
M-2 53	47	FB
M-2 60 FB	48	fixed bed tubular reactor (7.5 min growth)
M-2 60 FB	44	fixed bed tubular reactor (10 min growth)
M-2 60 FB	46	fixed bed tubular reactor (15 min growth)
M-3 19	55	FB

6 rpm and are in the range of 70–80° and 35–45°, respectively. Increasing the rotation speed above 6 rpm leads to a significant decrease in both the angle of avalanche and the angle of overhang. In the case of MWCNTs forming a stable fluidized bed, at a rotation speed of <10 rpm, a linear increase in the overhang angle from 10° to 30° is observed with a change in the angle of avalanche in the range of 60–65°. At a rotation speed of more than 10 rpm, there is a sharp decrease in both the avalanche angle and the overhang angle down to 45° and 20°, respectively.

3.4.4. Cohesion index of the MWCNT powders

Cohesion index of the MWCNT powders I_{coh} is determined through the ratio of the powder-air interface length L_{samp} to the boundary length

of the layer of the same volume of ideal powder with zero cohesion, L_{ideal} , calculated in advance from the data on the initial stationary powder volume:

$$I_{coh} = \left(\frac{L_{samp}}{L_{ideal}} - 1 \right) \cdot 100\% \quad (2)$$

Data on the cohesion index of MWCNT powders, I_{coh} , depending on the speed of rotation of the drum, ω , are presented in Fig. 11. As can be seen, these dependences are characterized by specific behavior for each of the three types of MWCNTs. Nanotubes forming a stable FB show a slight tendency for the cohesion index to increase from 15–40 to 40–60 as the drum speed increases (Fig. 11A). For MWCNTs forming unstable FB high values of the cohesion index (40–60) at low rotation speed of the drum sharply decrease to 10–15 with an increase in this speed at 30 rpm. For MWCNTs characterized by an intermediate tendency to form clumps, the dependence $I_{coh}(\omega)$ has a slightly pronounced extremum at $\omega = 3–5$ rpm, and at high speeds of rotation of the drum it behaves similarly to nanotubes with high cohesion.

It is important that such significant features in the behavior of cohesion index were observed in the range of linear velocities of powder movement in the drum rheometer close to the velocities of gas and agglomerates in the FB reactor. This means that the dynamic situation in a drum rheometer is rather close to that in the fluidized bed.

The demonstrated changes in the cohesion index with increasing drum rotation speed can be interpreted in terms of the energy balance between the ordered macroscopic motion of the nanotube layer (in this case, the energy of rotational motion), on the one hand, and the adhesive interaction of MWCNT agglomerates and the kinetic energy of their chaotic movement, on the other. The surface of a layer of agglomerates with weak cohesion is quite loose and grows weakly with increasing rotation speed due to the “stretching” of the layer by friction and centrifugal forces (Fig. 11A). In contrast, the layer of agglomerates with high cohesion is denser and more consolidated at low speeds of rotation of the drum, so that the cohesion index for this type of MWCNTs does not tend to increase with increasing rotational speed. The large nanotube agglomerates formed due to high cohesion begin to break down, and the layer surface becomes smoother with an increase in ω and, accordingly, the growth of kinetic energy of the layer (Fig. 11C). This is also clearly seen in the video recording of the behavior of the layer in the drum rheometer at various rotation speeds.

One more mechanism can be pointed out that promotes the growth of giant secondary agglomerates in a fluidized bed of a highly cohesive powder. Imagine that there is a region in the FB reactor with a high concentration of cohesive agglomerates. Inside this region, there is an active growth small agglomerates and their merging of into large ones, and the permeability of this region with respect to the blown gas becomes lower compared to the layer permeability at the initial moment. As a result of this effect, the velocities of the gas and particles in the region under consideration decrease, and therefore the kinetic energy of these particles becomes insufficient for the destruction of the formed

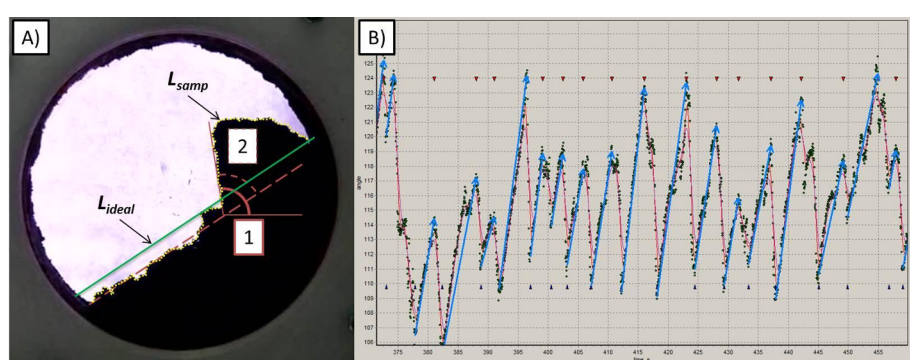


Fig. 9. A) Parameters of the analyzed MWCNT powder in drum rheometer experiments: 1 – the avalanche angle; 2 – the overhang angle; L_{samp} – the length of the powder-air interface in the sample; and L_{ideal} – the length of the powder-air interface for an ideal non-cohesive powder. B) The characteristic dependence of the avalanche angle on time for sample M-3 20; arrows indicate the moments of MWCNT accumulation before avalanches. Each MWCNT powder was characterized by the specific avalanche time at a fixed drum speed.

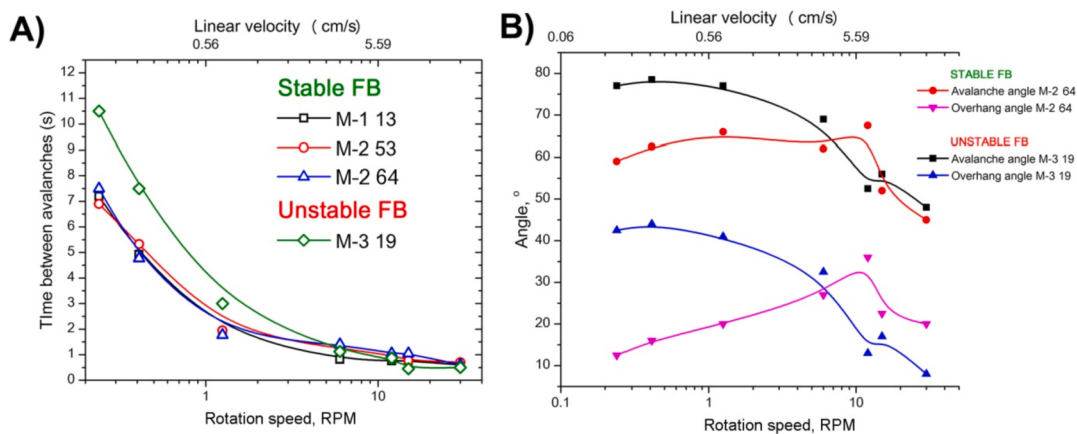


Fig. 10. A) Dependences of the time between avalanches on the rotation speed of the drum rheometer for different types of MWCNTs. B) Dependence of the angle of avalanche and angle of overhang on the rotation speed of the drum rheometer.

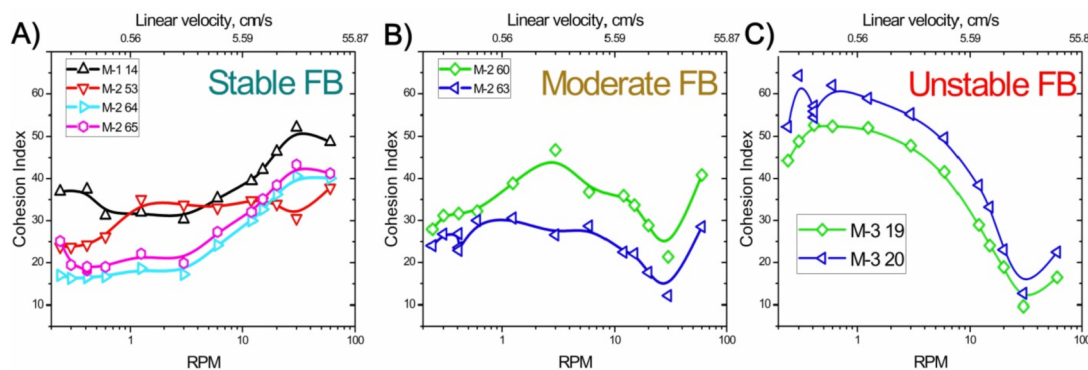


Fig. 11. Cohesion index of the MWCNT powders produced with different catalysts versus the drum rotation speed ("Stable FB", "Moderate FB" and "Unstable FB" correspond to the tendency to clump formation in FB reactor, see Table 1).

secondary agglomerates. Thus, conditions are created for the further growth of the large secondary agglomerates by adding new primary and secondary ones to them.

The most convenient way to register the moment of formation of MWCNT clumps in the FB reactor is monitoring the pressure drop across the fluidized bed. If the change in the pressure drop deviates from the normal monotonic growth, it means that the fluidization becomes unstable and it is necessary to use a special procedure to destroy the formed clumps of MWCNTs, i.e., to increase the gas flow through the reactor, purge the bed, or completely replace the MWCNTs that form the FB.

Summarizing the experimental methods for characterizing the cohesive properties of MWCNTs and the results of such characterization, it can be argued that the most indicative are the characteristics determined in a rotary rheometer, namely, the avalanche angle, overhang angle and cohesion index, as well as their dependence on the drum rotation speed. It is important to note that the most clumping MWCNT powders, during the synthesis of which plugging of the reactor was observed, were characterized by large angles of avalanche and overhang. The dependence of the volume of the MWNT layer on the speed of rotation of the drum rheometer is also a good indicator of the cohesive properties of agglomerates. For clumping MWCNT powders (obtained using the K-3 19 catalyst), the increase in the powder layer volume with an increase in the rotation speed of the rheometer drum up to 60 rpm was insignificant, which indicates a high stability of MWCNT agglomerates, i.e., their high cohesion. At the same time, for other MWCNTs that do not form large clumps in FB, an increase in the rotation speed of the rheometer drum led to a significant increase in volume, which corresponds to a relatively low cohesion of agglomerates of such nanotubes.

From the above experimental data, it can be concluded that the

formation of clumps and the loss of fluidization homogeneity during the catalytic synthesis of MWCNTs in a fluidized bed are caused by three factors: (i) the high cohesiveness of MWCNTs, (ii) the morphology and dispersibility of catalyst particles, and (iii) the catalyst particles number density in the FB. It seems interesting in theoretical and practical terms to estimate at least approximately the critical conditions under which the formation of large agglomerates of MWCNTs becomes a real problem in order to consciously deal with such situations in the future. In the next section, such a theoretical consideration is carried out on the basis of the well-known model of particle coagulation.

3.5. Coagulation model of the growth of large agglomerates during the catalytic synthesis of MWCNTs in a fluidized bed

3.5.1. A qualitative picture of large agglomerates formation

Based on the quantitative estimates that will be presented below, we propose the sequence of stages of the process leading to the formation of a large (global) agglomerate that disturbs the homogeneity of fluidization of MWCNT powder during the catalytic synthesis in a fluidized bed. It should be emphasized that the scheme of loss of fluidization for growing MWCNTs layer presented below is a simplified one because it does not take into account the continuing growth of primary agglomerates during coagulation processes, as well as the more subtle effects of collisions of secondary agglomerates of different sizes. However, the conclusions drawn from it turn out to be very close to the experimental data.

The formation of a large cluster can be thought of as the following sequence of stages.

1. The process begins with injection of a portion of fresh catalyst into the reactor with a fluidized bed of carbon nanotubes. The reactor was preliminarily heated to the required temperature (about 670 °C) and purged with a fluidizing inert gas (argon). Before the injection of the catalyst, the gas mixture containing a hydrocarbon precursor (ethylene) and argon is fed into the reactor. Fresh catalyst particles loaded into the reactor are uniformly distributed over the fluidized bed, simultaneously activated (i.e., metal-oxide nanoparticles in it are reduced to metals) and start to work in 100–150 s.
2. After the activation period, the catalyst particles are quickly covered with a “hedgehog” of nanotubes and become a primary agglomerate with high cohesive properties. These primary agglomerates stick together with each other and with the newly formed secondary agglomerates, ensuring their growth. Let us assume that the initial catalyst particles have sizes from 40 to 80 μm and their density is about 1000 kg/m³. We will also assume that the primary agglomerate is a spherical formation with a core in the form of a catalyst particle and a shell, which is a “hedgehog” of nanotubes. Taking into account the high productivity of the catalyst ($m_{nt,15\text{ min}}/m_c = 20$) [10], we may consider that the primary agglomerates grown on these particles have a density close to the known density of synthesized nanotubes, approximately 100 kg/m³ (per primary agglomerate, without taking into account the porosity of the bulk layer). If we also assume that the primary agglomerate is a spherical formation with a core in the form of a catalyst particle and a shell, which is a “hedgehog” of nanotubes, then it is easy to come to the following conclusions (details of the calculation are omitted due to their elementary nature): in 2–3 min after the beginning of the synthesis, a catalyst particle with the initial diameter of 40–80 μm turns into a primary agglomerate of nanotubes with the outer diameter of 120–220 μm. After that, the growth of the size of primary agglomerates slows down, and for an approximate simulation of the formation of a large agglomerate, we can assume the diameter of the primary agglomerates to be constant and equal to their average size reached during the specified period of fast growth.
3. The cohesive primary agglomerates, colliding with each other, form secondary agglomerates, but gradually, during the first 10 min of synthesis, the agglomerates lose their high cohesion as a result of surface “rolling”, which occurs in a fluidized bed. Thus, the formation of a global agglomerate of MWCNTs is possible only within no more than 10 min after loading the catalyst into the reactor.
4. The density of the large agglomerate decreases with its growth due to its fractality. However, due to the significant increase in size, the large agglomerate can reach such conditions when its suspended state in a fluidized bed becomes impossible. Then it either falls onto the gas distribution grid or “sticks” to the reactor wall. Such events lead to the disruption of homogeneous fluidization in the reactor and, often, to the termination of its normal operation.

The main idea of the model for the formation of a large (giant) agglomerate is that before the expiration of the initial 10-min period of high cohesiveness, the agglomerate must grow to such a size that no longer allows it to be in a fluidization state. Obviously, the formation time of a giant agglomerate depends on the frequency of collisions between primary agglomerates as well as between secondary agglomerates formed from them. Therefore, the main parameters affecting this process are the average distance between the catalyst particles after its loading into the fluidized bed and the speed of chaotic movement of the primary agglomerates of MWCNTs formed on these particles.

3.5.2. Coagulation kinetics of MWCNT primary and secondary agglomerates

To determine the conditions for the formation of a global agglomerate, we used the following approximate model based on the kinetics of primary agglomerate growth due to catalytic synthesis of MWCNTs and secondary agglomerates growth via binary collisions and coagulation of

the primary agglomerates, as well as newly formed secondary agglomerates.

The dynamics of the increase in the size of primary agglomerates can be described based on the data on the kinetics of the growth of MWCNTs, studied in [11]. For further approximate consideration, one can obtain a simple estimate for the agglomerate mass growth rate constant k : in 15 min, their mass increases approximately 20 times, i.e. $k = 0.022 \text{ s}^{-1}$. Assuming that the growth of the primary agglomerate begins on a catalyst particle with a diameter d_0 and the density ρ_{cp} , and that, in the limit of a long growth time, the density of the agglomerate tends to a certain final density of synthesized MWCNT primary agglomerate ρ_{pa} , we can find the dependence of the diameter of the primary agglomerate on time:

$$d_{ag,0} = d_0 \sqrt[3]{1 + k \frac{\rho_{cp}}{\rho_{pa}} t}. \quad (3)$$

In subsequent calculations, the following values of the indicated densities were used: $\rho_{cp} = 1000 \text{ kg/m}^3$ and $\rho_{pa} = 80 \text{ kg/m}^3$.

It was assumed that the primary agglomerates, as well as the secondary ones formed from them, retain high cohesive properties during approximately the first 10 min after the injection of a fresh portion of the catalyst into the reactor (see the previous Section). As a result of a series of successive collisions of these agglomerates, large agglomerates are formed and continue to grow, and their structure turns out to be fractal, which is common in coagulation processes. The mass of a fractal agglomerate grows proportionally to some degree of its radius ($M_{la} R_{la}^{d_f}$), where $d_f \leq 3$ is the fractal dimension of this agglomerate. According to numerous studies, typical values of d_f lie commonly between 1.7 and 2.5. For our estimates, we further used the value $d_f = 2.25$. Thus, the effective density of a large agglomerate decreases with an increase in the number of primary agglomerates constituting it:

$$\rho_{la} = \frac{M_{la}}{V_{la}} N_{la}^{1-\frac{3}{d_f}} \quad (4)$$

and the porosity of a large agglomerate is calculated as.

$$\varepsilon_{la} = 1 - \frac{\rho_{la}}{\rho_{pa}} \quad (5)$$

where N_{la} is the number of primary agglomerates in a large one, and ρ_{pa} is the density of the primary agglomerates. Fig. 12 illustrates that the porosity becomes very large when N_{la} increases.

An approximate calculation of the growth of large (global) agglomerates can be carried out rather easily if we assume that their formation occurs as a result of pairwise fusion of the particles containing the same number of primary agglomerates. In particular, we considered the following sequence of steps: first, single primary agglomerates form pairs, then these two-particle agglomerates combine in pairs to form particles containing four primary agglomerates, these particles merge

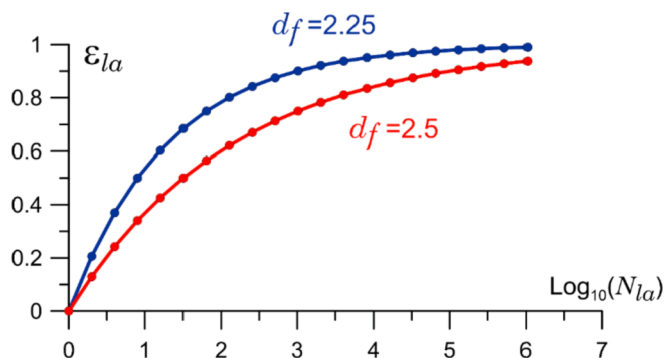


Fig. 12. Porosity of large agglomerates vs the number of primary agglomerates in it.

into the particles containing eight primary agglomerates, etc.

The approach based on the binary collision model for clusters of the same size uses the well-known expressions for the frequency of particle collisions in a fluidized bed [44–46]:

$$r_{agg} = 4\sqrt{2}\sqrt{D_i}\beta_0 n_i^2 \quad (6)$$

where n_i and D_i are the concentration and diameter of growing agglomerates formed after the i -th step of merging of primary agglomerates; and β_0 is the collision constant defined as:

$\beta_0 = \psi g_0 \sqrt{\frac{3\theta_s}{\rho_i}}$. In the last equation, ψ is the sticking factor (in calculations it is assumed that $\psi = 1$ due to high cohesion between primary agglomerates), $\theta_s = \frac{1}{3}m_i < C^2 >$ the modified kinetic temperature of a particle in a fluidized bed (common granular temperature multiplied by the particle mass) [47,44,45], $< C^2 >$ is the mean squared velocity of particle chaotic motion in FB, ρ_i is the density of agglomerate formed after i -th step of merging, $g_0(\varepsilon_s)$ is the radial distribution function, $g_0(\varepsilon_s) = \frac{2-\varepsilon_s}{2(1-\varepsilon_s)^3}$, and ε_s is the volume fraction of a solid in FB (defined by the volume of macroscopic particles, namely primary agglomerates).

Using this kinetics of binary collision, we arrive at the expression for the time of complete coagulation of agglomerates of i -th generation:

$$\tau_i = \frac{n_i}{2r_{agg}} \quad (7)$$

As a result of the sequence of the considered binary collisions, agglomerates of ever larger sizes are formed, but with a gradually decreasing density. The growth process of large agglomerates gradually slows down and ends in about 10 min due to a decrease in the cohesive properties of the agglomerates. As an agglomerate grows, the number of primary agglomerates in it grows too, and the minimum gas velocity required for its fluidization becomes higher. The condition when the loss of fluidization for large agglomerate occurs is the excess of minimal fluidization velocity over the velocity of the fluidizing gas, which must be reached within the specified time period of 10 min.

To illustrate the above considerations, calculations were performed for three catalysts described in Fig. 6 (Section 3.3). These catalysts differ in their fractional composition. The first catalyst, K-2 64 (<40 μm), has the smallest size and the number of its particles in the 0.5 g loaded portion is $80 \cdot 10^6$, while the other two catalysts (K-2 63 (40–80 μm) and K-2 64 (40–80 μm)) consist of larger particles and, as a consequence, their numerical concentrations are lower, especially for the second catalyst K-2 63, ($5 \cdot 10^6$). For this reason, the distance between the catalyst particles, and hence between the primary agglomerates, as well as the frequency of their collisions will be higher. Fig. 13 shows how the size and density of large clusters change over time depending on the size of the initial catalyst particles when the same masses of catalysts are loaded into the reactor. The limiting size of the large agglomerate, at which it can be suspended in a fluidized bed, is shown in the figure by the horizontal dashed line. This maximum size of the agglomerates that can be fluidized at a given gas velocity (0.1 m/s, argon-ethylene mixture, temperature 670 °C in considering example) was calculated using the well-known condition for minimum fluidization velocity ([48], p. 69). It is clearly seen that the agglomerates formed on catalyst # 1, which has the minimum size and the maximum numerical density in the fluidized bed, reach the limiting diameter in a short time after the start of MWCNT synthesis on a fresh catalyst, approximately equal to 3 min. However, the coagulating agglomerates formed on the other two catalysts do not reach the critical size of defluidization during the time at which high cohesion of the primary agglomerates is maintained. Thus, the most important condition determining the loss of homogeneous fluidization during the catalytic synthesis of MWCNTs in a fluidized bed is the size and number density of the catalyst particles when the catalyst is loaded into the reactor.

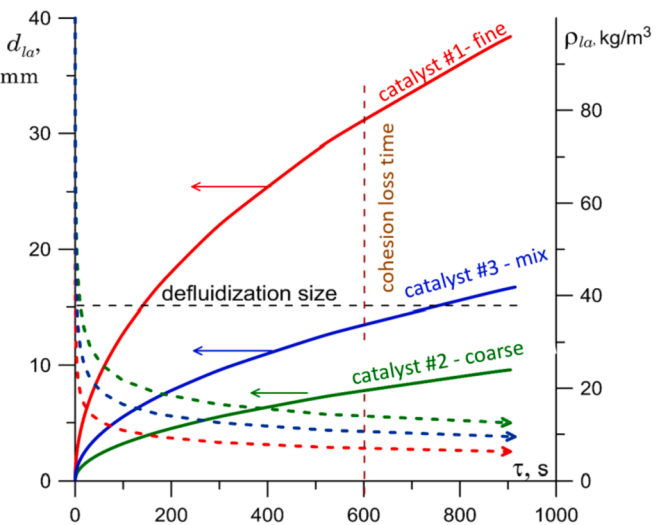


Fig. 13. Growth of the size of large agglomerates (solid lines) and their density (dashed lines) due to coagulation processes during the initial time period after catalyst loading into the FB reactor. Agglomerates formed on the first catalyst have a time to gain the critical size of defluidization, whereas the second and third catalysts generate agglomerates with a lower concentration in the FB, which continue to be in a fluidized state.

4. General discussion and conclusions

According to measurements of the Hausner ratio, angle of repose, angles of avalanche and overhang, and cohesion index, the MWCNT M-3 powders demonstrated the lowest flowability. The SEM study on the structure of nanotube agglomerates revealed an essential difference in the surface morphology of nanotube agglomerates obtained with the use of K-1(2) and K-3 catalysts. It was found that the surface of MWCNT agglomerates obtained using K-1 and K-2 catalysts is covered with the entangled bundles of nanotubes. Such bundles have a relatively low rigidity and can easily bend upon collision of the agglomerates. On the contrary, the surface of MWCNT agglomerates produced on the K-3 catalyst is covered with individual nanotubes of a greater diameter (~20 nm) as compared to agglomerates obtained on K-1(2) catalysts (7–10 nm). Due to their greater diameter, these nanotubes are more rigid and less bent. This promotes the formation of primary agglomerates with a relatively low density due to chaotic orientation of the growing nanotubes in the agglomerates. In addition, more rigid nanotubes can penetrate quite easily into the bulk of primary agglomerates during their collisions, thus facilitating the growth of clumps in the FB-reactor.

The above analysis of the experimental data on the conditions for the loss of homogeneity of the fluidized bed of MWCNTs during their catalytic synthesis, as well as the theoretical estimates based on the concept of coagulation growth of large MWCNT clusters, showed that the main reason for defluidization in the MWCNT synthesis reactor is the formation and growth of large MWCNT agglomerates during the initial period of synthesis on a fresh catalyst to such sizes that make it impossible for them to remain in a fluidized state. The formation of such large agglomerates of MWCNTs is a consequence of the high cohesion of the primary agglomerates formed during the synthesis and depends, first of all, on the concentration of growth centers (catalyst particles) in the fluidized bed. An excessively high concentration of the growth centers may be caused by a too small particle size of the catalyst loaded into the reactor (at a fixed weight of the charge), or it may arise as a result of the dispersion of a larger catalyst particles that occurs during the first period of MWCNT growth. Of course, the entire formation process of large agglomerates of MWCNTs occurs against the background of a very strong cohesion of the primary agglomerates of MWCNTs, which, within certain limits, can be controlled by choosing the catalyst composition

and morphology.

The critical concentration of the catalyst during its loading into the reactor can be estimated on the basis of the coagulation model and information on the growth kinetics of primary agglomerates of MWCNTs.

The reduction in the concentration of the catalyst particles is especially important in the initial period of time after loading a new portion of the catalyst into the reactor. Therefore, one of the recipes for solving the problem of a loss of FB homogeneity is fractional loading of the catalyst in small portions with a short (from 15 to 120 s) time interval between their injection into the fluidized bed.

A solution to the problem for a highly dispersible catalyst (K-3) was found by analogy with the processes of gas-phase polymerization of ethylene and propylene using a prepolymer with an active catalyst. So, to obtain a stable fluidized bed in the case of a highly dispersing catalyst K-3, it was mixed in a knife mill with the previously obtained MWCNTs (in a 1:1 ratio). This made it possible to achieve stable operation of the reactor with the FB (more than 25 SR cycles without complete reloading and cleaning of the reactor).

Thus, the main requirements for the morphology of catalysts and the organization of the synthesis process for solving the problem of continuous and large-scale production of MWCNTs in FB reactors have been formulated. On the one hand, this ensures the synthesis of MWCNTs with specified characteristics (diameter, specific area) by controlling the microstructure of the catalyst and optimizing the SR cycles, which makes it possible to control the size of MWCNT agglomerates, and on the other hand, it provides maximum productivity and conversion of the initial gaseous reagent [11].

Declaration of Competing Interest

The authors declare that they have no known competing financial interests or personal relationships that could have appeared to influence the work reported in this paper.

Acknowledgments

The work was carried out with the financial support of the Russian Foundation for Basic Research (project No. 20-53-00031) and the Belarusian Republican Foundation for Fundamental Research (project No. T20R-349).

Appendix A. Supplementary data

Supplementary data to this article can be found online at <https://doi.org/10.1016/j.cej.2022.137391>.

References

- [1] Industrial Applications of Carbon Nanotubes, Eds.; Huiheng Peng, Qingwen Li and Tao Chen, 2017 Elsevier Inc., Amsterdam, Oxford, Cambridge, ISBN: 978-0-323-41481-4.
- [2] NT21: International Conference on the Science and Application of Nanotubes and Low-Dimensional Materials, June 6–11, 2021. Rice University, Houston, USA. <https://dryfta-assets.s3.eu-central-1.amazonaws.com/assets/nt21/editorimages/1625712328NT21-abstract-book-A4.pdf>.
- [3] Yu Hao, Zhang Qunfeng, Wei Fei, Qian Weizhong, Luo Guohua, Agglomerated CNTs synthesized in a fluidized bed reactor: Agglomerate structure and formation mechanism, Carbon 41 (2003) 2855–2863, [https://doi.org/10.1016/S0008-6223\(03\)00425-1](https://doi.org/10.1016/S0008-6223(03)00425-1).
- [4] A. Firoozeh Danafar, Mohd Amran Fakhrul-Razi, Mohd Salleh, Dayang Radiah Awang Biak, Fluidized bed catalytic chemical vapor deposition synthesis of carbon, nanotubes—A review, Chem. Eng. J. 155 (2009) 37–48, <https://doi.org/10.1016/j.cej.2009.07.052>.
- [5] Gui-Li Tian, Jia-Qi Huang, Jun Li, Qiang Zhang, Fei Wei, Enhanced growth of carbon nanotube bundles in a magnetically assisted fluidized bed chemical vapor deposition, Carbon 108 (2016) 404–411, <https://doi.org/10.1016/j.carbon.2016.07.036>.
- [6] K. Dasgupta, J.B. Joshi, S. Banerjee, Fluidized bed synthesis of carbon nanotubes – A review, Chem. Eng. J. 171 (2011) 841–869, <https://doi.org/10.1016/j.cej.2011.05.038>.
- [7] R. Smajda, J.C. Andresen, M. Duchamp, R. Meunier, S. Casimirius, K. Hernádi, L. Forró, A. Magrez, Synthesis and mechanical properties of carbon nanotubes produced by the water assisted CVD process, Physica status solidi (b) 246 (2009) 2457–2460, <https://doi.org/10.1002/pssb.200982269>.
- [8] A. Magrez, J.W. Seo, R. Smajda, M. Mionić, L. Forró, Catalytic CVD synthesis of carbon nanotubes: towards high yield and low temperature growth, Materials 11 (2010) 4871–4891, <https://doi.org/10.3390/ma3114871>.
- [9] A. Usoltseva, V. Kuznetsov, N. Rudina, E. Moroz, M. Haluska, S. Roth, Influence of catalysts' activation on their activity and selectivity in carbon nanotubes synthesis, Physica Status Solidi (b) 244 (11) (2007) 3920–3924, <https://doi.org/10.1002/pssb.200776143>.
- [10] O. Rabinovich, A. Tsytsevna (Blinova), V. Kuznetsov, S. Moseenkov, D. Krasnikov, A Model for Catalytic Synthesis of Carbon Nanotubes in a Fluidized-Bed Reactor: Effect of Reaction Heat, Chem. Eng. J. 329 (2017) 305–311, <https://doi.org/10.1016/j.cej.2017.06.001>.
- [11] O.S. Rabinovich, V.A. Borodulya, A.N. Blinova, V.L. Kuznetsov, A.I. Delidovich, D. V. Krasnikov, Simulation of transient processes of the catalytic synthesis of carbon nanotubes in a fluidized bed, Theor. Found. Chem. Eng. 48 (1) (2014) 1–14, <https://doi.org/10.7868/S0040357114010114>.
- [12] D.V. Krasnikov, V.L. Kuznetsov, A.O. Romanenko, A.N. Shmakov, Side Reaction in Catalytic CVD Growth of Carbon Nanotubes: Surface Pyrolysis of a Hydrocarbon Precursor with the Formation of Lateral Carbon Deposits, Carbon 139 (2018) 105–117, <https://doi.org/10.1016/j.carbon.2018.06.033>.
- [13] Y. Wang, Y. Cheng, Y. Jin, H.T. Bi, On impacts of solid properties and operating conditions on the performance of gas-solid fluidization systems, Powder Technol. 172 (2007) 167–176.
- [14] J.M. Valverde Millán, in: Fluidization of fine powders: cohesive versus dynamical aggregation, Springer, 2012, p. 134.
- [15] D. Geldart, Types of gas fluidization, Powder Technol. 7 (5) (1973) 285–292, [https://doi.org/10.1016/0032-5910\(73\)80037-3](https://doi.org/10.1016/0032-5910(73)80037-3).
- [16] https://en.catalysis.ru/block/index.php?ID=27&SECTION_ID=1686.
- [17] A.I. Romanenko, O.B. Anikeeva, T.I. Buryakov, E.N. Tkachev, K.R. Zhdanov, V. L. Kuznetsov, I.N. Mazov, A.N. Usoltseva, A.V. Ischenko, Influence of Surface Layer Conditions of Multiwall Carbon Nanotubes on Their Electrophysical Properties, Diam. Relat. Mater. 19. N7–9 (2010) 964–967, <https://doi.org/10.1016/j.diamond.2010.02.035>.
- [18] M.I. Bagatskii, A. Jeżowski, D. Szewczyk, V.V. Sumarovov, M.S. Barabashko, V. L. Kuznetsov, S.I. Moseenkov, A.N. Ponomarev, Size Effects in the Heat Capacity of Modified MWCNTs, 101097:1–6, Therm. Sci. Eng. Prog. 26 (2021), <https://doi.org/10.1016/j.tsep.2021.101097>.
- [19] K. Pikula, A. Zakharenko, V. Chaika, I. Em, A. Nikitina, E. Avtomonov, A. Tregubenko, A. Agoshkov, I. Mishakov, V. Kuznetsov, A. Gusev, S. Park, K. Golokhvast, Toxicity of Carbon, Silicon, and Metal-Based Nanoparticles to Sea Urchin Strongylocentrotus Intermedius, Nanomaterials 10 (9) (2020) 1–11, <https://doi.org/10.3390/nano10091825>.
- [20] V.L. Kuznetsov, S.N. Bokova-Sirosh, S.I. Moseenkov, A.V. Ishchenko, D. V. Krasnikov, M.A. Kazakova, A.I. Romanenko, E.N. Tkachev, E.D. Obraztsova, Raman spectra for characterization of defective CVD multi-walled carbon, nanotubes, Phys. Status Solidi B 251 (2014), <https://doi.org/10.1002/pssb.201451195>, 2444e2450.
- [21] V.L. Kuznetsov, K.V. Elumeeva, A.V. Ishchenko, N.Y. Beylina, A.A. Stepashkin, S. I. Moseenkov, L.M. Plyasova, I.Y. Molina, A.I. Romanenko, O.B. Anikeeva, E. N. Tkachev, Multi-Walled Carbon Nanotubes with ppm Level of Impurities, Phys. Status Solidi (B): Basic Res. 247. N11–12 (2010) 2695–2699, <https://doi.org/10.1002/pssb.201000211>.
- [22] K.V. Elumeeva, V.L. Kuznetsov, A.V. Ischenko, R. Smajda, M. Spina, L. Forro, A. Magrez, Reinforcement of CVD Grown Multi-Walled Carbon Nanotubes by High Temperature Annealing, P.112101-1-8, AIP Adv. 3 (2013), <https://doi.org/10.1063/1.4829272>.
- [23] I. Mazov, V.L. Kuznetsov, I.A. Simonova, A.I. Stadnichenko, A.V. Ishchenko, A. I. Romanenko, E.N. Tkachev, O.B. Anikeeva, Oxidation Behavior of Multiwall Carbon Nanotubes with Different Diameters and Morphology, Appl. Surf. Sci. 258. N17 (2012) 6272–6280, <https://doi.org/10.1016/j.apsusc.2012.03.021>.
- [24] A.I. Romanenko, O.B. Anikeeva, T.I. Buryakov, E.N. Tkachev, K.R. Zhdanov, V. L. Kuznetsov, I.N. Mazov, A.N. Usoltseva, Electrophysical Properties of Multiwalled Carbon Nanotubes with Various Diameters, Phys. Status Solidi (B): Basic Res. 246. N11–12 (2009) 2641–2644, <https://doi.org/10.1002/pssb.200982267>.
- [25] G.R. Karagedov, R.A. Shutilov, B.A. Kolesov, V.L. Kuznetsov, The Effect of Carbon Nanotubes Introduction on the Mechanical Properties of Reaction Bonded Boron Carbide Ceramics, J. Eur. Ceram. Soc. 41. N12 (2021) 5782–5790, <https://doi.org/10.1016/j.jeurceramsoc.2021.05.014>.
- [26] A.V. Zavorin, V.L. Kuznetsov, S.I. Moseenkov, T.-O. Tsendsure, V.A. Volodin, P. S. Galkin, A.V. Ishchenko, Chemical Vapor Deposition of Silicon Nanoparticles on the Surface of Multiwalled Carbon Nanotubes, J. Struct. Chem. 61. N4 (2020) 617–627, <https://doi.org/10.1134/S0022476620040162>.
- [27] R.A. Shutilov, V.L. Kuznetsov, S.I. Moseenkov, G.R. Karagedov, A.A. Krasnov, P.V. Logachev, Vacuum-Tight Ceramic Composite Materials Based on Alumina Modified with Multi-Walled Carbon Nanotubes, Materials Science and Engineering B: Solid-State Materials for Advanced Technology (Materials Science and Engineering B-Advanced Functional Solid-State Materials). 2020. V.254. 114508:1–10. DOI: 10.1016/j.mseb.2020.114508.
- [28] I.N. Mazov, I.A. Illyukh, V.L. Kuznetsov, A.A. Stepashkin, K.S. Ergin, D.S. Muratov, V.V. Tcherdyntsev, D.V. Kuznetsov, J.-P. Issi, Thermal Conductivity of Polypropylene-Based Composites with Multiwall Carbon Nanotubes with Different Diameter and Morphology, J. Alloy. Compd. 586 (Suppl. 1) (2014) S440–S442, <https://doi.org/10.1016/j.jallcom.2012.10.167>.

- [29] I.N. Mazov, V.L. Kuznetsov, S.I. Moseenkov, A.V. Ishchenko, A.I. Romanenko, O.B. Anikeeva, T.I. Buryakov, E.Y. Korovin, V.A. Zhuravlev, V.I. Suslyaev, Electrophysical and Electromagnetic Properties of Pure MWNTs and MWNT/PMMA Composite Materials Depending on Their Structure, Fullerenes, Nanotubes, Carbon Nanostruct. 18. N4–6 (2010) 505–515, <https://doi.org/10.1080/1536383X.2010.488184>.
- [30] [30] J.Macutkevic, P. Kuzhir, A. Paddubskaya, M. Shuba, J. Banys, S. Maksimenko, V.L. Kuznetsov, I.N. Mazov, D.V. Krasnikov, Influence of Carbon-Nanotube Diameters on Composite Dielectric Properties, Physica Status Solidi (A) Applications and Materials (after 2004). 2013. V.210. N11. P.2491-2498. DOI: 10.1002/pssa.201329254.
- [31] J. Macutkevic, D. Seliuta, G. Valusis, R. Adomavičius, A. Krotkus, P. Kuzhir, A. Paddubskaya, S. Maksimenko, V. Kuznetsov, I. Mazov, I. Simonova, Multi-Walled Carbon Nanotubes/PMMA Composites for THz Applications, Diam. Relat. Mater. 25 (2012) P.13-18, <https://doi.org/10.1016/j.diamond.2012.02.002>.
- [32] A.G. Selyutin, A.N. Shmakov, V.L. Kuznetsov, S.I. Moseenkov, D.V. Dudina, O. I. Lomovsky, Characterization of Aluminum-Carbon Composites Obtained via Mechanical Activation of Aluminum and Carbon Nanotubes, Bulletin of the Russian Academy of Sciences: Physics. 77. N1 (2013) 162–165, <https://doi.org/10.3103/S1062873813020329>.
- [33] M. P. Pechini, Method of preparing lead and alkaline earth titanates and niobates and coating method using the same to form a capacitor, US Patent 3,3306,97. 1967.
- [34] V.L. Kuznetsov and A.N. Usoltseva, A method for the preparation of highly dispersed deposited catalysts and the synthesis of carbon nanotubes, Patent RF No. 2373995, 27.11.2009.
- [35] V.L. Kuznetsov, D.V. Krasnikov, A.N. Schmakov, K.V. Elumeeva, In situ and ex situ time resolved study of multi-component Fe-Co oxide catalyst activation during MWNT synthesis, Phys. Status Solidi B 249 (12) (2012) 2390–2394. DOI 10.1002/pssb.201200120.
- [36] D.V. Krasnikov, S.N. Bokova-Sirosh, T.-O. Tsendsuren, A.I. Romanenko, E. D. Obraztsova, V.A. Volodin, V.L. Kuznetsov, Influence of the Growth Temperature on the Defective Structure of the Multi-Walled Carbon Nanotubes, Phys. Status Solidi (B): Basic Res. 255 (1) (2018) 1–6, <https://doi.org/10.1002/pssb.201700255>.
- [37] T. Mckenna, Condensed Mode Cooling of Ethylene Polymerization in Fluidized Bed Reactors, in: Macromolecular Reaction Engineering, Wiley-VCH Verlag, 2019, p. 1800026, hal-01980513.
- [38] H.H. Hausner, Powder characteristics and their effect on powder processing, Powder Technol. 30 (1) (1981) 3–8, [https://doi.org/10.1016/0032-5910\(81\)85021-8](https://doi.org/10.1016/0032-5910(81)85021-8).
- [39] ASTM International (2009) ASTM D7481-09, standard test methods for determining loose and tapped bulk densities of powders using a graduated cylinder. ASTM International, West Conshohocken, PA.
- [40] A.S. Andreev, D.V. Krasnikov, V.I. Zaikovskii, S.V. Cherepanova, M.A. Kazakova, O.B. Lapina, V.L. Kuznetsov, J. d'Espinouse de Lacaille, Internal Field 59 Co NMR Study of Cobalt-Iron Nanoparticles During the Activation of CoFe2/CaO Catalyst for Carbon Nanotube Synthesis, J. Catal. 358 (2018) P.62-70, <https://doi.org/10.1016/j.jcat.2017.11.025>.
- [41] A.B. Yu, J.S. Hall, Packing of fine powders subjected to tapping, Powder Technol. 78 (3) (1994) 247–256, [https://doi.org/10.1016/0032-5910\(93\)02790-H](https://doi.org/10.1016/0032-5910(93)02790-H).
- [42] E.C. Abdullah, D. Geldart, The use of bulk density measurements as flowability indicators, Powder Technol. 102 (2) (1999) 151–165, [https://doi.org/10.1016/S0032-5910\(98\)00208-3](https://doi.org/10.1016/S0032-5910(98)00208-3).
- [43] A.B. Spiersings, M. Voegtlín, T. Bauer, K. Wegener, Powder flowability characterisation methodology for powder-bedbased metal additive manufacturing, Prog. Addit. Manuf. 1 (2016) 9–20, <https://doi.org/10.1007/s40964-015-0001-4>.
- [44] M. Goldschmidt, Hydrodynamic Modelling of Fluidised Bed Spray Granulation, University of Twente, 2001, p. 319. Ph.D. thesis.
- [45] H.S. Tan, A.D. Salman, M.J. Hounslow, Kinetics of fluidized bed melt granulation—II: Modelling the net rate of growth, Chem. Eng. Sci. 61 (2006) 3930–3941, <https://doi.org/10.1016/j.ces.2006.01.005>.
- [46] K.W. Chua, Y.T. Makkawi, M.J. Hounslow, A priori prediction of aggregation efficiency and rate constant for fluidized bed melt granulation, Chem. Eng. Sci. 98 (2013) 291–297, <https://doi.org/10.1016/j.ces.2013.05.018>.
- [47] D. Gidaspow, Multiphase flow and fluidization: continuum and kinetic theory descriptions, Academic Press, 1994, p. 474.
- [48] D. Kunii, O. Levenspiel, Fluidization Engineering, Butterworth—Heinemann, Boston, 1993, ISBN 0-409-90233-0.